

Supplemental information

**CD4⁺ T-cell-derived IL-10 promotes CNS inflammation
in mice by sustaining effector T cell survival**

Nir Yoge, Tanja Bedke, Yasushi Kobayashi, Leonie Brockmann, Dominika Lukas, Tommy Regen, Andrew L. Croxford, Alexei Nikolav, Nadine Hövelmeyer, Esther von Stebut, Marco Prinz, Carles Ubeda, Kevin J. Maloy, Nicola Gagliani, Richard A. Flavell, Ari Waisman, and Samuel Huber

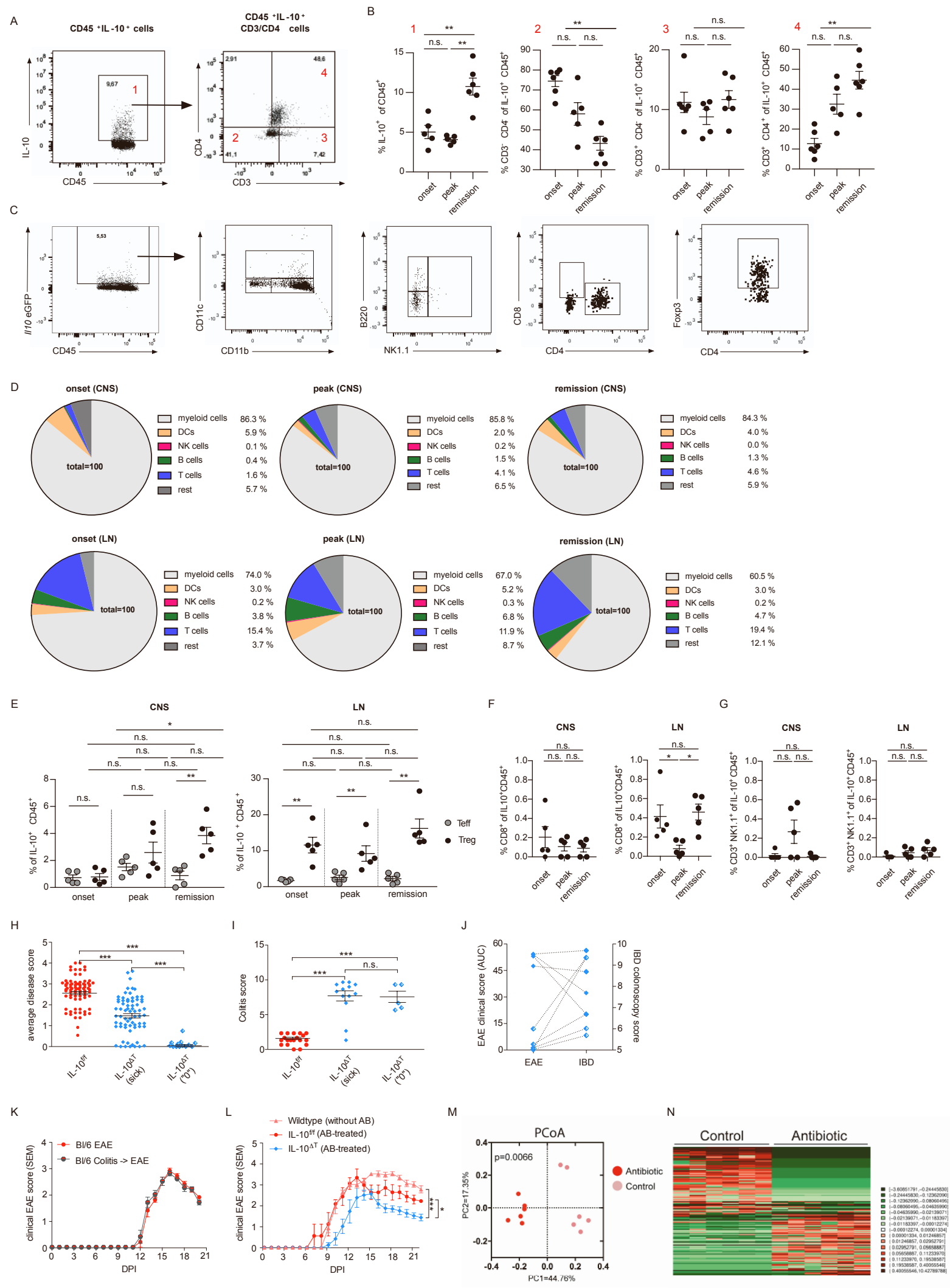


Figure S1

Figure S1 related to Figure 1: EAE mediated immune cell-derived IL-10 production and extra-intestinal inflammation.

(A, B) Lymphocytes were isolated from the CNS of wild-type mice with an EAE score of 1.5 (onset, d11), 3 (peak, d15), and 2.5 after (remission, d23) and restimulated with PMA/Ionomycin in the presence of Monensin for 5 hours prior antibody staining for CD45, CD3, CD4, and IL-10. (A) Representative Dotplots of IL-10⁺CD45⁺ cells (left) and IL-10⁺CD3⁺CD4⁺ (right) at disease remission. (B) Graphs summarize the percentage of CNS-infiltrating IL-10⁺CD45⁺ leukocytes (1) IL-10⁺CD3⁻CD4⁻ (2) IL-10⁺CD3⁺CD4⁻ (3), and IL-10⁺CD3⁺CD4⁺ (4) cells isolated from 5 mice per time-point. (C) Analysis of *Il10eGFP* expression by CD45⁺ leukocyte populations using the following gating strategy: CD45⁺IL-10⁺ cells (left) were subdivided into myeloid cells (CD11b⁺CD11c⁻); DCs (CD11c⁺CD11b^{+/−}); B cells (NK1.1[−]B220⁺); NK cells (B220[−]NK1.1⁺); CD8 T cells (CD4[−]CD8⁺); CD4⁺Foxp3⁺ (Treg), and CD4⁺Foxp3[−] (Teff). (D-G) Graphs summarize the percentage of the analyzed IL-10⁺ cell populations isolated from the CNS and LN at the indicated time points. Data represent mean \pm SEM of $n = 5$ per condition obtained from 2 independent experiments. For statistical analysis Kruskal-Wallis was used. (H) EAE disease score in both *CD4*^{Cre.neg}/*Il10*^{f/f} control (IL-10^{f/f}) and *CD4*^{Cre.pos}/*Il10*^{f/f} (IL-10^{ΔT}) mice. Both IL-10^{f/f} and IL-10^{ΔT} (sick) mice developed EAE score of ≥ 2 that lasted for two days or longer. IL-10^{ΔT} (“0”) mice on the other hand, developed EAE score of ≤ 1 that lasted for two days or less. (I) Colitis disease score of individual IL-10^{f/f} and IL-10^{ΔT} animals. Representative animals were randomly selected among those analyzed for EAE development (shown in H). (J) EAE/Colitis correlative incidence analysis among representative individual IL-10^{ΔT} animals. (K) EAE disease curve of either C57BL/6 (Bl/6 EAE) or C57BL/6 mice that were previously subjected to DSS-induced colitis (Bl/6 Colitis \rightarrow EAE). (L) EAE disease curve in IL-10^{f/f} and IL-10^{ΔT} mice that have been maintained on broad-antibiotic treatment starting from the gestational stage and throughout their entire life span as well as control mice which has not received any antibiotic treatment. (K-L) Representative disease curve of ≥ 2 experiments, shown as mean \pm SEM of $n \geq 8$ per group. (M, N) Mice treated for three consecutive weeks with sulfadoxin-trimethoprim in the drinking water. As control, another group of mice did not receive

antibiotics. Fecal samples were collected three weeks after treatment initiation. The microbiota was analysed through 16s rRNA high-throughput sequencing. (M) Principal coordinate of analysis based on Bray-curtis distances at the level of amplicon sequence variants (ASV). The p value indicates that both groups have a significantly different microbiota composition ($p<0.05$, PERMANOVA test). (N) Heatmap showing the amplicon sequence variants whose abundance significantly differs between both groups of mice (ANCOM2 & FDR, $q<0.05$). For each ASV, the mean relative abundance was calculated. Then, for each sample, the original relative abundance was normalized as the difference respect to the mean of the corresponding ASV.

Supplementary Table 1 related to Figure 1: 16S rRNA sequence analysis of the gut microbiota.

Taxonomy and q values obtained for each amplicon sequence variants (ASV). For each ASV, the mean relative abundance was calculated. Then, for each sample, the original relative abundance was normalized as the difference respect to the mean of the corresponding ASV. The obtained value represented with a colour as depicted. The taxonomy and q values obtained for each ASV are shown.

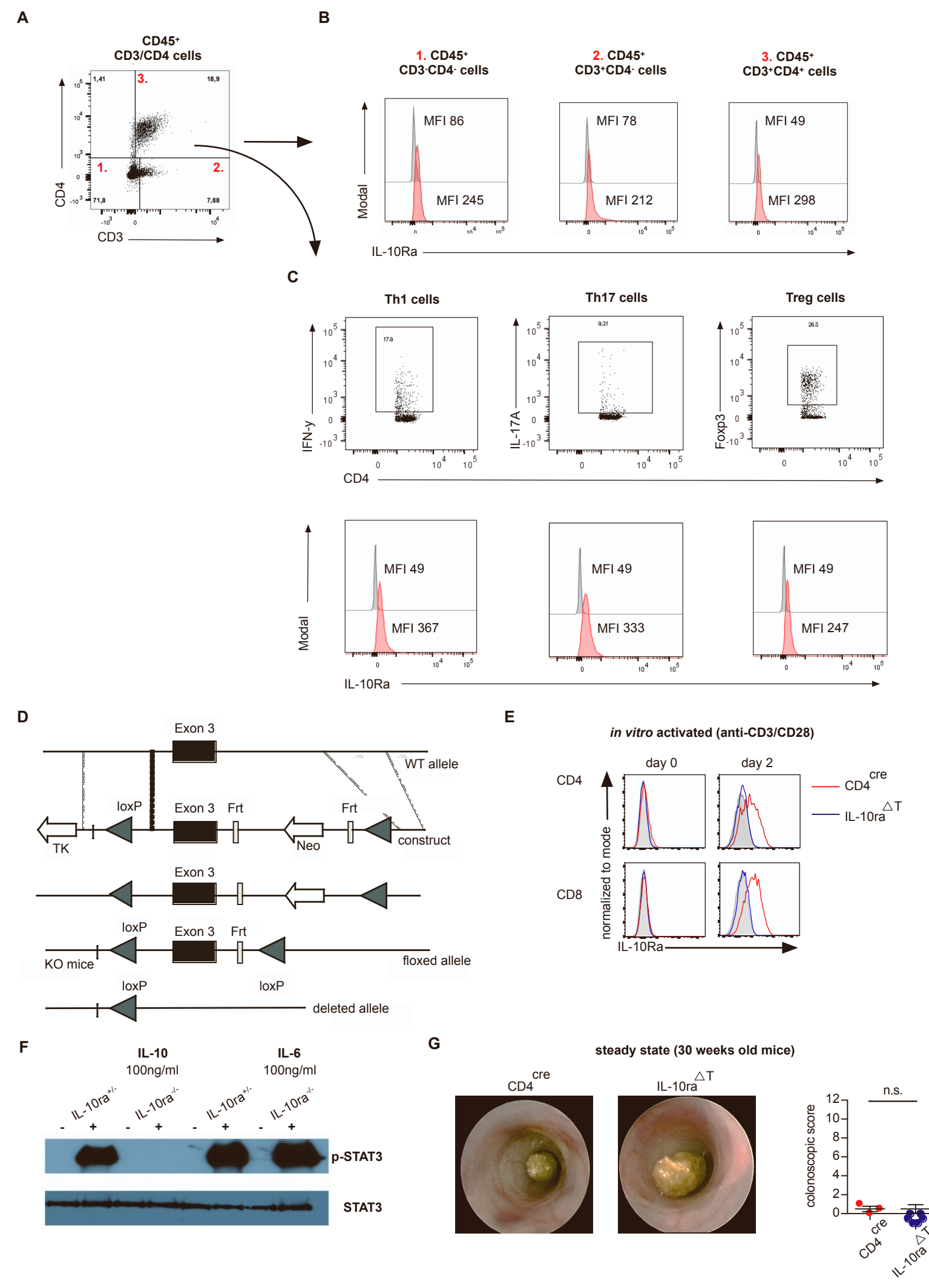


Figure S2

Figure S2 related to Figure 2: Gating strategy for the identification of IL10Ra expressing immune cells and characterization of $CD4^{Cre}/IL10ra^{fl/fl}$ mice.

(A) Gating strategy of IL10 receptor expression: CD45⁺ cells (not shown) were first subdivided into CD3⁻CD4⁻, CD3⁺CD4⁻, and CD3⁺CD4⁺ cell subsets. (B) Histograms show FMO for IL-10R staining (grey) of the indicated subset overlayed with IL-10R staining (red) of the same subset. (C) Gating of *Ifng* FP635⁺ Th1 cells, *Il17a* eGFP⁺ Th17 cells and *Foxp3* RFP⁺ Treg cells from CD3⁺CD4⁺ (as shown in A). lower Panel: Histograms show FMO for IL-10R staining (grey) of CD4⁺ T cells overlayed with IL-10R staining (red) of the indicated subset. (D) *Il10ra* construct used for the generation of $CD4^{Cre}/IL10ra^{fl/fl}$ mice. (E) IL-10R α expression on CD4⁺ T cells and CD8⁺ T cells directly after isolation from spleens of untreated $CD4^{Cre}/IL10ra^{wt/wt}$ ($CD4^{Cre}$) and $CD4^{Cre}/IL10ra^{fl/fl}$ (IL-10R $\alpha^{\Delta T}$) mice and after 2 days of *in vitro* activation in the presence of 1 μ g/ml soluble anti-CD3 and anti-CD28 mAb. (F) Western blot of STAT3 phosphorylation of CD4⁺ T cells isolated from heterozygous $CD4^{Cre}/IL10ra^{fl/wt}$ and $CD4^{Cre}/IL10ra^{fl/fl}$ (IL-10R $\alpha^{\Delta T}$) mice after *in vitro* stimulation with 100 ng/ml IL-10 or 100 ng/ml IL-6 as a positive control, respectively. (G) Endoscopy of 30 weeks old untreated CD4^{Cre} and IL-10R $\alpha^{\Delta T}$ mice as described in material and methods.

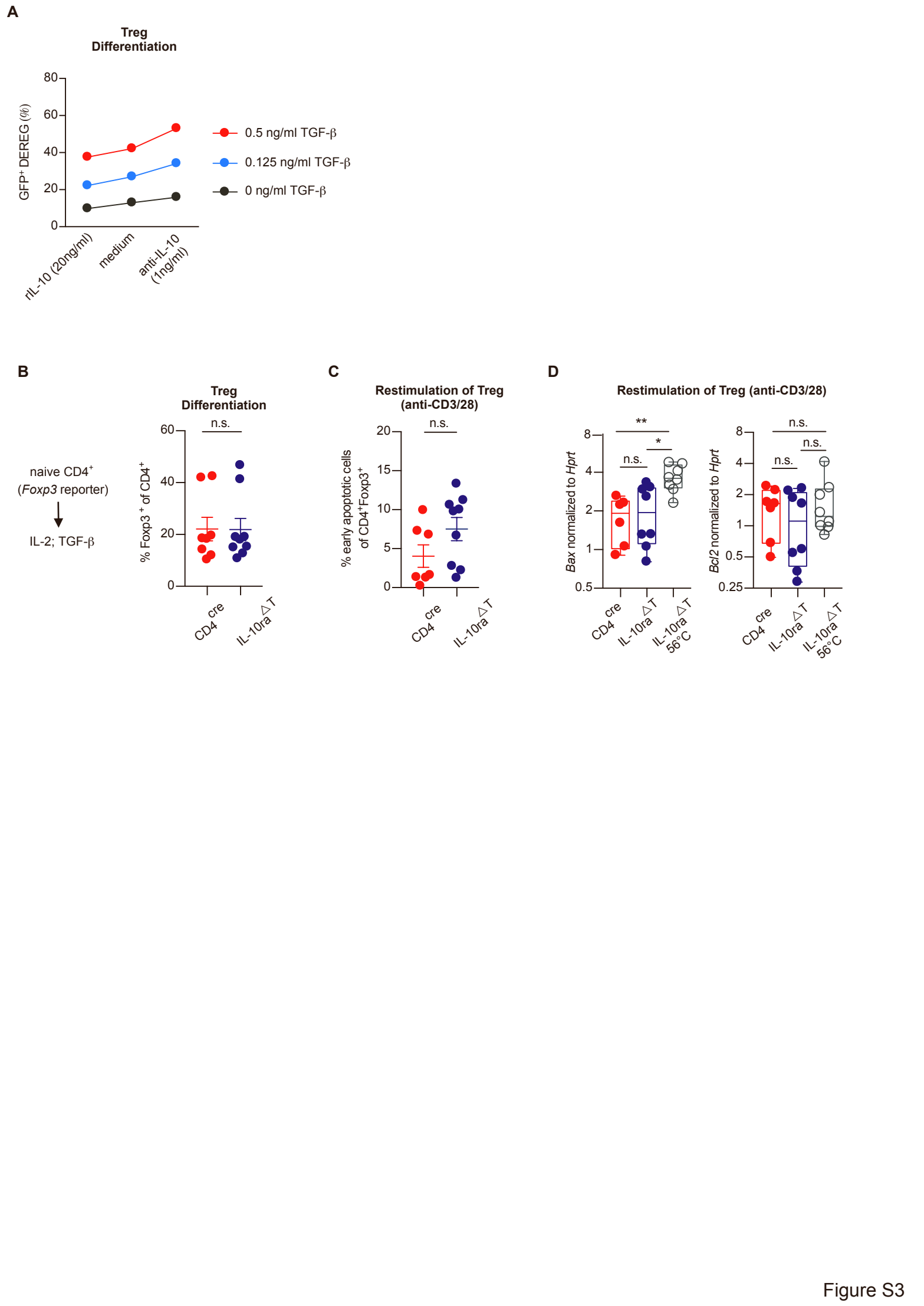


Figure S3

Figure S3 related to Figure 3: IL-10 signaling in Treg is dispensable for their survival *in vitro*.

(A) FACS sorted naïve CD4 T cells, isolated from the FoxP3-GFP reporter mice were plated on 96 well plate (2×10^5 /well, triplicates) in serum free/TGF β -free medium. Cells were stimulated with anti CD3/CD28, TGF β at the indicated concentrations, and treated with either rIL-10 (20ng/ml), anti-IL-10 (1 μ g/ml) or without further stimuli. 72hrs post stimulation, the triplicates were pooled, stained and analyzed by FACS. Data shown as percentages of GFP $^+$ iTreg of total viable CD4 $^+$ T cells. One representative experiment of two. (B) Flow cytometric analysis of the frequencies of induced *Foxp3* RFP $^+$ Treg after 5 days of *in vitro* differentiation from naïve IL10R $\alpha^{\Delta T}$ T cells (blue; n=9) and CD4 Cre CD4 $^+$ T cells (red; n=8). (C) FACS analysis of early apoptotic Annexin $^+$ Pacific Orange $^-$ iTreg (left) and (D) mRNA expression levels of the pro-apoptotic gene *Bax* and anti-apoptotic gene *Bcl2* in sorted IL-10R $\alpha^{\Delta T}$ and CD4 Cre iTreg after 16hr (for FACS analysis) and 12 hrs (for qPCR analysis) of restimulation with plate-bound 1 μ g/ml anti-CD3 and soluble anti-CD28 mAb. Grey bars show gene expression after heat induced apoptosis induction as positive control.

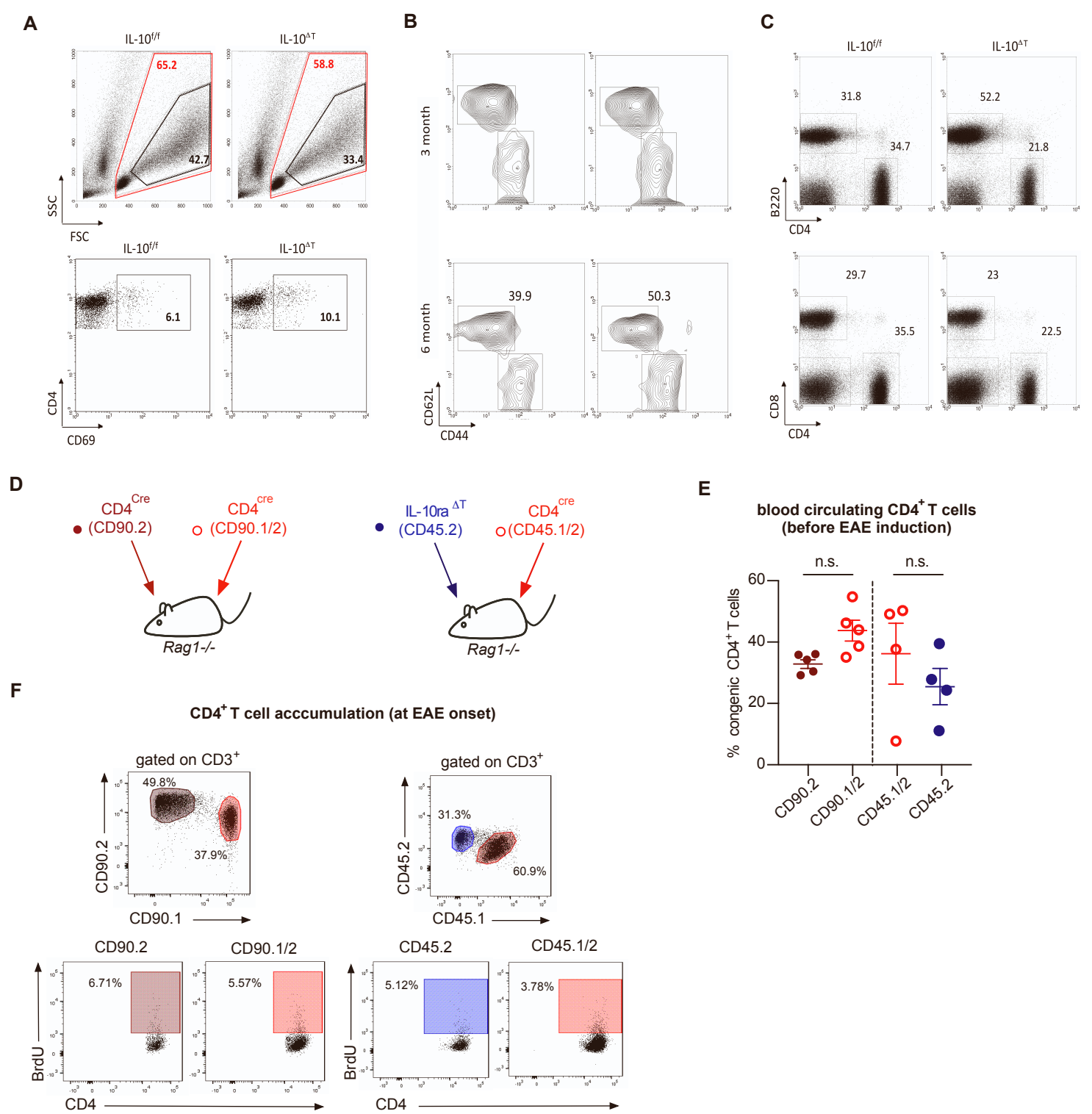


Figure S4

Figure S4 related to Figure 4: Loss of effector *Il10*-deficient T cells *in vivo* and reconstitution efficiency after co-transfer of *Il10ra*-proficient and -deficient T cells into *Rag1*^{-/-} mice.

(A) MACS-enriched CD4⁺ T cells isolated from ing.LN of EAE mice (day 10-post immunization) and co-cultured with MOG₃₅₋₅₅-pulsed BMDCs, IL-2, IL-12 and IL-23 for 5 days. (Upper panel) percentage of total viable cells (red) or cell-blasts (black). (Lower panel) percentage of activated (CD69⁺) CD4⁺ T cells. (B) Percentage of naïve CD4⁺ T cells found in LN of healthy, non-challenged, young and old mice (3 vs 6 month-old, respectively). (C) B cell (B220⁺) to CD4⁺ T cell ratio (upper panel), and CD8⁺ to CD4⁺ T cell ratio (lower panel), as seen in healthy, non-challenged, young mice. (D) Experimental layout of CD4⁺ T cell co-transfer into *Rag1*^{-/-} mice: Co-transfer of CD4⁺ T cells derived from littermate control mice (*CD4*^{Cre}/*Il10ra*^{wt/wt}, short CD4^{Cre}), expressing either CD90.2 or CD90.1/2 congenic marker (dark red, full circles red vs red, empty circles, respectively). (right) Co-transfer of CD4⁺ T cells derived from either CD4^{Cre} control and IL-10r<α^{ΔT} mice or littermate CD4^{Cre} control mice, expressing either CD45.2 or CD45.1/2 congenic marker (blue, full circle vs red, empty circle, respectively). (E) To determine the reconstitution efficiency of congenic CD4^{Cre} wild-type and IL-10r<α^{ΔT} CD4⁺ T cells peripheral blood was sampled 4 to 5 weeks after reconstitution and stained for CD4, CD90.1 and CD90.2 or CD4, CD45.1 and CD45.2, respectively. The Diagram shows the ratio of congenic CD4⁺ T cells after transfer of a mixture of equal numbers of CD4^{Cre}:CD4^{Cre} control cells (left) and after transfer of a mixture of equal numbers of IL-10r<α^{ΔT}:CD4^{Cre} control cells (right). (F) After 4 to 5 weeks of reconstitution, the mice were immunized with MOG₃₅₋₅₅ as described in the Material and Methods section, and gating strategy of FACS analyses of T cell subpopulations were performed at the indicated time points, as shown here for BrdU staining. Co-transfer of CD4⁺ T cells derived from littermate control mice (*CD4*^{Cre, pos}/*Il10ra*^{wt/wt}, short CD4^{Cre}), expressing either CD90.2 (brown) or CD90.1/2 (red) congenic marker (also labeled as full vs empty circles, respectively). (right) Co-transfer of CD4⁺ T cells derived from IL-10r<α^{ΔT} and CD4^{Cre} control mice, expressing either CD45.2 (blue) or CD45.1/2 (red) congenic marker (also labeled as full vs empty circle, respectively).